

# The Adjoint of CMAQ

AMIR HAKAMI <sup>1</sup>, DAVEN K. HENZE <sup>1</sup>, JOHN H. SEINFELD <sup>1</sup>, KUMARESH SINGH <sup>2</sup>, ADRIAN SANDU <sup>2</sup>, SOONTAE KIM <sup>3</sup>, DAEWON BYUN <sup>3</sup>, QINBIN LI <sup>4</sup>

<sup>1</sup> Department of Chemical Engineering, California Institute of Technology, Pasadena, California.

5 <sup>2</sup> Department of Computer Science, Virginia Polytechnic Institute and State University, Blacksburg, Virginia.

<sup>3</sup> Geosciences Department, University of Houston, Houston, Texas.

<sup>4</sup> Tropospheric Modeling and Analysis, Jet Propulsion Laboratory, Pasadena, California.

**ABSTRACT.** An adjoint model for the internationally used Community Multiscale Air Quality (CMAQ) modeling platform of the U.S. EPA is developed. The adjoint version for CMAQ (CMAQ-ADJ) provides the user community with forward (direct decoupled method or DDM) and backward (adjoint) sensitivity analysis capabilities. Current implementation is for gas-phase processes. Discrete adjoints are implemented for all processes with the exception of horizontal advection, for which, because of inherent discontinuities in the advection scheme, the continuous approach is superior. The adjoint of chemistry is constructed by interfacing CMAQ with the Kinetic Pre-Processor (KPP), which provides for increased flexibility in choice of chemical solver and facilitates implementation of new chemical mechanisms. The adjoint implementation is evaluated both on a process-by-process basis and for the full model. In general, adjoint results show good agreement with brute-force and DDM sensitivities. As expected for a continuous adjoint implementation in a nonlinear scheme, the agreement is not perfect for horizontal transport. Sensitivities of various air quality, public health, and environmental metrics with respect to emissions are calculated using the adjoint method. In order to

show applicability to regional climate studies, as an example, sensitivities of these metrics with respect to local temperatures are calculated.

## **Introduction**

25 Three-dimensional atmospheric chemical transport models (CTMs) are used to predict spatial and temporal distributions of airborne pollutants. In recent years, they have been increasingly modified to provide information, not only about concentrations, but also sensitivities of atmospheric levels with respect to various parameters. Owing in part to increased computational resources, sensitivity analysis has received more attention and new methods have been developed to more efficiently calculate  
30 sensitivity coefficients (derivatives) of model outputs with respect to various inputs. Sensitivity information provided by atmospheric models can be used in various applications such as design of optimal pollution control strategies, inverse modeling and model parameter estimation, and air quality forecasting and data assimilation.

35 Local sensitivity analysis techniques can be divided into two general categories of forward and backward methods. In the often-used forward method, sensitivities are propagated forward (along the model trajectories) from the perturbed source into various receptors/outputs (1-3). By nature, the methods in this category are efficient in simultaneously providing sensitivity information about all receptors with respect to a few specific parameters (4-7). In backward (adjoint) sensitivity analysis, the  
40 perturbation is made at the receptor end and is propagated backward in time and space through an auxiliary set of equations. As a result, adjoint sensitivity analysis provides simultaneous sensitivity information about specific receptors with respect to all sources and parameters.

Adjoint sensitivity analysis in its current form can be traced back to the early stages of nuclear reactor  
45 physics in 1940s and 1950s (comprehensive views on the history of the adjoint method for sensitivity analysis are given in 8, 9). Adjoint sensitivity analysis was later applied to various environmental

problems (10-15). In particular, it has been used extensively in meteorology and oceanography for various applications such as sensitivity analysis (16, 17), variational data assimilation (18-20), parameter estimation (21), etc. In the last decade, adjoint analysis has been extended to three-dimensional CTMs. Elbern *et al.* (22-25) developed an adjoint for the EURAD CTM and performed chemical data assimilation and inverse modeling of emissions. Vukicevic and Hess (26) implemented the adjoint method in the tracer model HANK and performed sensitivity analysis with respect to various parameters. More recently, adjoint versions for other global or regional CTMs have been developed for various applications such as inverse modeling and sensitivity analysis; these include regional models CHIMERE (27-29), STEM (30-32), Polair (33-34), CIT (35, 36), and DRAIS (37), and global models IMAGES (38, 39), TM4 (40), and GEOS-Chem (41). However, among the regional and air quality models for which an adjoint version is available, none is widely used in the modeling community. In this work, we develop an adjoint for the Community Multiscale Air Quality (CMAQ) model of U.S. EPA (42, 43). CMAQ is generally considered as the most widely used regional air quality model in the U.S. and across the world. Furthermore, we demonstrate how the adjoint model can be used for sensitivity analysis of various air quality and/or environmental metrics. The adjoint method, in tandem with DDM, provides the users of CMAQ with a powerful set of analysis tools that can tackle a wide spectrum of problems.

## 65 **Development of the Adjoint**

Atmospheric Chemical Transport Models (CTMs) are based on the atmospheric diffusion equation (44, 45),

$$\frac{\partial C_i}{\partial t} = -\mathbf{u} \cdot \nabla C_i + \frac{1}{\rho} \nabla \cdot (\rho \mathbf{K} \nabla C_i) + R_i + E_i \quad (1)$$

70 where  $C_i$  is the mixing ratio of species  $i$  (a function of three-dimensional space and time),  $\mathbf{u}$  is the vector wind field,  $\mathbf{K}$  is the diffusivity tensor,  $E_i$  represents elevated emissions,  $\rho$  is the air density, and  $R_i$  is the net chemical reaction rate for the species. Equation (1) is solved subject to specified initial and

boundary conditions. In operator notation, the model operator matrix,  $M$ , maps the input parameters vector  $\alpha$  (including initial conditions) into the output domain,

75

$$\mathbf{C} = \mathbf{M}\alpha \quad (2)$$

where  $C$  is the concentration vector at the end of the integration period ( $t_F$ ). For most common applications, principal input parameters are initial and boundary concentrations and emission rates, but they may also include other parameters such as chemical reaction rate constants, dry deposition velocities, etc. Equation (1) and the operator  $M$  can be referred to as the *forward model* and operator, respectively. Note that owing to nonlinearity in gas-phase chemistry,  $M$  is a nonlinear operator. Transport processes (horizontal and vertical advection and diffusion) in Equation (1), on the other hand, are physically linear processes, although these terms may be integrated numerically by nonlinear schemes in the discretized form.

85

A perturbation in the input parameters (e.g., emissions  $\delta E_i$ ) in Equation (1) results in a perturbation in each predicted concentration,  $\delta C_i$ , which is governed by,

$$\frac{\partial \delta C_i}{\partial t} = -\mathbf{u} \cdot \nabla (\delta C_i) + \frac{1}{\rho} \nabla \cdot (\rho \mathbf{K} \nabla \delta C_i) + \mathbf{F}_i \delta \mathbf{C} + \delta E_i \quad (3)$$

90 where  $\mathbf{F}_i$  is the  $i$ th row of the Jacobian of the chemical reaction rates ( $F_{ij} = \partial R_i / \partial C_j$ ). Equation (3) can be represented in operator form as,

$$\delta \mathbf{C} = \mathbf{L} \delta \alpha \quad (4)$$

where  $L$  is the Jacobian of the model operator at the base case conditions. Equations (3) and (4) represent the linearized form of the forward model/operator, and are referred to as the Tangent Linear Model (TLM) and operators, respectively. Note that Equation (3) is also equivalent to the system of sensitivity equations solved in the direct decoupled method (DDM) (2, 3) for sensitivity analysis; TLM

and DDM can be used interchangeably to refer to the forward method for calculation of first-order local (in the sense of a small perturbation) sensitivity coefficients,  $\delta C_i/\delta E_j$ .

100

If one defines a scalar cost function of the concentration field computed by the model (forms of the cost function for problems of interest in the application of CMAQ are discussed in Section 4) as,

$$J = \iint_{t,\omega} g(\mathbf{C}, t, \omega) d\omega dt \quad (5)$$

105

where  $\omega$  is the generalized spatial coordinate, then an *adjoint model* to the TLM/DDM can be derived by applying Lagrange multipliers and integration by parts to Equation (3) and its associated initial and boundary conditions,

$$-\frac{\partial \lambda_i}{\partial t} = \nabla \cdot (\mathbf{u} \lambda_i) + \nabla \cdot \left( \rho \mathbf{K} \nabla \frac{\lambda_i}{\rho} \right) + \mathbf{F}_i^T \boldsymbol{\lambda} + \varphi_i \quad (6)$$

110

where  $\mathbf{F}_i^T$  is the  $i$ th row of the transposed Jacobian (or the transpose of the  $i$ th column of the original Jacobian) of the chemical reaction rates,  $\lambda_i$  is the adjoint variable for species  $i$  such that at each time and location  $\lambda_i = \partial J / \partial C_i$ , and  $\varphi_i$  is the forcing term for the adjoint equations,

$$\varphi_i = \frac{\partial g}{\partial C_i} \quad (7)$$

115

Details of the derivation of adjoint equations and related initial and boundary conditions for a CTM can be found in Elbern et al., (2000), Sandu et al., (2005), Hakami et al. (2005), Martien et al. (2006), and Henze et al. (2007). Equation (6) is challenging to solve owing to the concentration-dependent cost function and the associated forcing term,  $\varphi_i$ . The negative sign preceding the transient term in Equation (6) indicates that the adjoint equations are integrated backwards in time. Calculation of the Jacobian of the reaction rates in Equations (3) and (6) requires values of the state vector (concentrations). For TLM/DDM calculations this is achieved easily, as the integrations for the TLM/DDM and forward models may be advanced together. For adjoint calculations, however, concentrations need to be stored

120

(so-called *checkpointed*) in forward simulations and then used for backward integration. Checkpointing is also necessary for any other nonlinear process that is simulated in the backward mode.

125

The TLM/DDM equations are driven/forced by perturbations in the inputs/sources [e.g.,  $\delta E$  in Equation (3)]. These perturbations are then propagated forward in time to produce a field of sensitivity coefficients with respect to the perturbed input/source parameter. On the other hand, the forcing terms for the adjoint equations are perturbations in a scalar, receptor-based cost function [i.e.,  $\varphi_i$  in Equation (6)] that are propagated backward in time. Therefore, integration of the adjoint equations results in a field of sensitivity coefficients of the cost function with respect to model inputs. TLM/DDM is a source-based forward sensitivity method suitable for calculating sensitivities of a large number of outputs with respect to a few inputs. Adjoint sensitivity analysis, on the other hand, is a receptor-based, backward method that is most efficient in calculating sensitivities of a few outputs with respect to numerous inputs. The duality in the range of efficiency and applicability for forward (TLM/DDM) and backward (adjoint) sensitivity analysis methods makes them complementary approaches for addressing a wide spectrum of problems.

130

135

The adjoint of a linear operator  $L$  can also be defined using the following duality principle,

140

$$\langle \mathbf{u}, \mathbf{L}\mathbf{v} \rangle_n = \langle \mathbf{L}^* \mathbf{u}, \mathbf{v} \rangle_n \quad (8)$$

where  $L^*$  is the adjoint operator, and  $\langle \cdot, \cdot \rangle_n$  denotes the inner product in  $R^n$ . Applying Equation (8) to the TLM/DDM model:

145

$$\langle \delta \mathbf{C}, \mathbf{L} \delta \mathbf{a} \rangle = \langle \mathbf{L}^* \delta \mathbf{C}, \delta \mathbf{a} \rangle \quad (9)$$

Or:

$$(\mathbf{L} \delta \mathbf{a})^T (\mathbf{L} \delta \mathbf{a}) = \delta \mathbf{a}^T \mathbf{L}^* (\mathbf{L} \delta \mathbf{a}) \quad (10)$$

which can be used for verification of the adjoint operator from a validated TLM/DDM model (46).

150

Two approaches exist for integration of the adjoint equations. In the continuous approach, the adjoint Equations (6) are discretized and solved numerically. Alternatively, discrete adjoint models may be developed directly from the discretized DDM model. The two approaches in general produce different results, as adjoint and discretization operations are not commutable (47). Note that the same distinction can be made between continuous and discrete approaches for development of TLM/DDM models.

155

In Equations (2) and (4) it is assumed that evolution of concentrations or sensitivities is described by a single operator. In practice, CTMs use an operator splitting scheme, and they also integrate the governing equations over multiple time steps. The overall operator can be considered as the composition of all internal steps. In other words, for a model of  $N$  time-steps and  $m$  processes at each step,

160

$$M = \left( M_{p_1}^1 \circ M_{p_2}^1 \circ \dots \circ M_{p_m}^1 \right) \circ \dots \circ \left( M_{p_1}^N \circ M_{p_2}^N \circ \dots \circ M_{p_m}^N \right) \quad (11a)$$

$$L = \left( L_{p_1}^1 \circ L_{p_2}^1 \circ \dots \circ L_{p_m}^1 \right) \circ \dots \circ \left( L_{p_1}^N \circ L_{p_2}^N \circ \dots \circ L_{p_m}^N \right) \quad (11b)$$

$$L^* = \left( L_{p_m}^N \right)^T \circ \left( L_{p_{m-1}}^N \right)^T \circ \dots \circ \left( L_{p_1}^N \right)^T \circ \dots \circ \left( L_{p_m}^1 \right)^T \circ \left( L_{p_{m-1}}^1 \right)^T \circ \dots \circ \left( L_{p_1}^1 \right)^T \quad (11c)$$

165

### Implementation of the Adjoint (CMAQ-ADJ)

In this work adjoint (and DDM) methods are implemented in CMAQ version 4.5.1 for gas-phase processes. (For identification purposes, this code is referred to as CMAQ-ADJ). As there are no significant changes in these processes in the recently released version 4.6, the adjoint model implementation can be equally applied to CMAQ 4.6. We use a hybrid approach in development of the adjoint (and DDM) model(s), wherein discrete adjoints for chemistry, diffusion, and vertical advection, and continuous adjoints for horizontal advection are employed. As explained later, these choices are made based on accuracy of the adjoints, as well as their physical significance.

170

175 A variation of DDM (4, 7) has been previously implemented in CMAQ (48). Implementation of  
DDM is briefly addressed to complement the discussion of adjoint implementation. The previous  
implementation of DDM in CMAQ employed a continuous approach. In the present DDM  
implementation a discrete approach for chemistry integration is used to enhance accuracy (see  
discussion on the chemistry adjoint below). Complete validation of the DDM results is not shown here,  
180 but in general they are in good agreement with brute-force finite difference calculations (Figure 1). Note  
that minor disagreements between DDM and brute-force results in Figure 1 are primarily a result of the  
use of a continuous approach for calculating DDM sensitivities of horizontal advection. Using a discrete  
approach for horizontal advection will enhance agreement between brute-force (BF) and DDM, but may  
produce physically inconsistent results (see discussion on horizontal advection below). The same  
185 problem will occur in vertical advection for earlier versions of CMAQ where a nonlinear scheme was  
employed.

Validating DDM results with BF sensitivities is a rather straightforward task as they both provide  
forward sensitivity fields. Validation of adjoint results can not be achieved as easily. For each pair of  
190 forward (DDM or BF) and backward (adjoint) sensitivity simulations, there is only one point-of-  
comparison available for validation purposes. Depending on the definition of the forward sensitivity  
parameter (perturbed source) and adjoint cost function (perturbed receptor), the point-of-comparison  
can be the sensitivity of a single output or an integrated concentration metric to changes in a single  
input or collective change to a set of inputs. Regardless of the source and receptor metrics involved,  
195 available points-of-comparison between each pair of forward and backward sensitivity fields is reduced  
to a single scalar. Therefore, a complete validation of adjoint variables for all locations, times, and  
species is pragmatically infeasible. In the following sections we describe the methods used for  
implementation of adjoint analysis in CMAQ, and then for validation purposes we will introduce  
reduced models where points-of-comparison between forward and backward sensitivity fields are  
200 increased. For example, for chemistry validation, forward and backward simulations are carried out only



for chemistry (transport processes turned off). Therefore, the 3-D model can be considered as an ensemble of numerous box models, each of which provides a point-of-comparison. The reduced chemistry-only model will then provide a three-dimensional (in space only) field of points-of-comparison between forward and backward sensitivity fields.

205

**Chemistry Adjoint.** In order to implement forward and backward sensitivity analysis capabilities, the Kinetic PreProcessor (KPP) version 2.2 (49, 50) has been integrated into CMAQ. KPP can be efficiently used to generate required subroutines for any chemical mechanism. Recent versions of KPP have been extended to include DDM and adjoint sensitivity analysis capabilities (51-53). KPP significantly enhances the flexibility of CMAQ for using new or modified chemical mechanisms. Chemical solvers offered in KPP are generic and independent of mechanism, and therefore, migration to a new chemistry can be achieved seamlessly. The latest version of KPP offers a choice from multiple Rosenbrock (54, 55) and Runge-Kutta solvers (including families of fully-implicit three-stage, and singly diagonally-implicit Runge-Kutta methods, see 56), where within each family various solvers differ in accuracy and stability properties. KPP generates all required subroutines for continuous and discrete DDM and adjoint sensitivity calculations. In general, KPP solvers compare favorably with CMAQ's SMVGEAR (57), ROS3, and Euler backward iterative (EBI) (58) solvers. At the default tolerance values, cpu time requirement for KPP's Rosenbrock solvers are comparable with EBI and lower than CMAQ's SMVGEAR and ROS3 (Table 1). Work-precision diagrams (55) for model simulations with original CMAQ solvers, as well as those of KPP are shown in Figure 2. These diagrams suggest that KPP's Rosenbrock solvers provide fairly accurate solutions at relatively low computational cost and outperform original CMAQ solvers.

State vectors (concentrations) are checkpointed at synchronization (chemistry) time steps into netCDF files. Currently, checkpointing is available only for fixed time steps in each simulation day. Therefore, predetermined synchronization steps are set for each day. Checkpoints are written during the forward

225

simulations. During the backward simulations, checkpointed concentrations are read at the beginning of each synchronization time step. The required checkpoints at the internal chemistry time steps are recalculated by forward integration of the concentrations for the synchronization time step (i.e., two-  
 230 level checkpointing, see 30, 59). Calculated chemistry-only adjoint sensitivities are in close agreement with BF values (Figure 3).

**Horizontal advection adjoint.** CMAQ version 4.5 uses the Piecewise Parabolic Method (60) to integrate the flux form of the one-dimensional horizontal advection equation,

$$235 \quad \frac{\partial(\eta)}{\partial t} = -\frac{\partial(u\eta)}{\partial x} \quad (12)$$

where  $\eta$  is the mass-based concentration vector ( $\eta = \rho C$ , where  $\rho$  is air density). If total mass continuity holds for the advection process, then Equation (12) is equivalent to:

$$240 \quad \frac{\partial C}{\partial t} = -u \frac{\partial C}{\partial x} \quad (13)$$

Applying a mass-based adjoint variable (for conservation) to Equation (13) results in the following one-dimensional adjoint advection equation,

$$-\frac{\partial(\lambda_m)}{\partial t} = \frac{\partial(u\lambda_m)}{\partial x} \quad (14)$$

245 where  $\lambda$  and  $\lambda_m$  are mixing ratio and mass-based adjoint variables ( $\lambda_m = \lambda/\rho$ ). Therefore, the one-dimensional adjoint advection equations solved in the continuous adjoint implementation are,

$$-\frac{\partial(\lambda/\rho)}{\partial t} = \frac{\partial(u\lambda/\rho)}{\partial x} \quad (15)$$

where all Dirichlet boundary conditions for the adjoints are set to zero. In forward simulations mixing  
 250 ratios are “coupled” with (multiplied by) densities (i.e., they are converted to mass-based concentrations) for advection processes. Subsequently, after the completion of each advection step, mass-based concentrations are “decoupled” from (divided by) densities and converted back to mixing

ratios. Unlike the forward calculations, in the backward simulation, conversion of mixing ratio to mass-based adjoints is accomplished by division by densities (see Table 2 for an operational scheme of the forward and backward simulations).

Figure 4 shows comparisons between adjoint and BF horizontal advection sensitivities. The simulations for Figure 4 include only horizontal advection in the  $x$ -direction, where the figure shows an  $x$ -cross section (for 23 vertical layers) of sensitivities of ozone at the final time step in the 20<sup>th</sup> column of the domain with respect to initial ozone concentrations in the 20<sup>th</sup> column. By considering advection in the  $x$ -direction as the sole process, a two-dimensional field of point-of-comparison between forward and backward sensitivity fields is available for visualization. BF sensitivities are calculated by various changes to the initial ozone at the 20<sup>th</sup> column. As can be seen, the general features of the advected fields are similar, but there are noticeable differences between the forward and backward fields. The adjoint field is smoother while negative sensitivities in the BF field are physically meaningless; negative sensitivities represent only numerical noise in the BF fields. The behavior seen in Figure 4 is consistent with previous studies of the adjoints of nonlinear advection schemes (41, 61, 62). Also note that BF fields are inconsistent among themselves (for various perturbations), and deviate further from the backward field for smaller perturbations. This indicates that differences between BF and adjoint fields are not a result of nonlinearities in the advection scheme, as they increase with decreasing perturbations. These differences instead result from discontinuity and non-differentiability in the forward scheme that causes irrecoverable inconsistencies between BF simulations (63). If a discrete adjoint approach is employed in these simulations, the resulting adjoint field would resemble a noisy BF sensitivity field. As a result of these inconsistencies, we conclude that for the current nonlinear advection scheme in CMAQ, continuous adjoint implementation of the horizontal advection scheme is superior to discrete implementation.

**Vertical advection adjoint.** CMAQ uses an upwind first order finite difference scheme for solving the vertical advection equation,

280

$$\frac{\partial(\eta)}{\partial t} = -\frac{\partial(w\eta)}{\partial z} \quad (16)$$

In CMAQ version 4.5, vertical advection is used as a mass conservation step. During horizontal advection, air densities are also advected alongside concentrations. In each ensuing vertical advection step, the vertical wind profile is calculated such that transported air density for that time step at each level matches meteorological densities from MM5. The calculated vertical wind profile is then applied to all species. It is necessary to use a similar vertical wind profile during backward calculations to that used in the forward simulations. Therefore, either transported air densities after each horizontal advection step or the calculated vertical wind profile at each vertical advection step during forward simulations need to be checkpointed.

290

Similar to horizontal advection, the corresponding adjoint equation for vertical advection is,

$$-\frac{\partial(\lambda/\rho)}{\partial t} = \frac{\partial(w\lambda/\rho)}{\partial z} \quad (17)$$

The same numerical subroutine may be used with the reverse vertical wind profile (continuous adjoint). In our implementation a discrete adjoint is developed for the linear scheme used in vertical advection. Applying the adjoint (transpose) of the linear operator above (discrete adjoint) yields different results than using the forward operator with the reverse wind profile (continuous adjoint). The discrete adjoint provides results that are more consistent with BF sensitivities (Figure 5). Note that in previous versions of CMAQ (before v4.5) where a nonlinear scheme is used for vertical advection, a continuous approach would be preferable.

300

**Vertical diffusion adjoint.** CMAQ provides an option for species emissions to be processed during chemistry or vertical diffusion integrations. In the present adjoint implementation, emissions are injected during vertical diffusion for which the following equation is solved,

305 
$$\frac{\partial C}{\partial t} = \frac{\partial}{\partial z} \left( K \frac{\partial C}{\partial z} \right) \quad (18)$$

with the corresponding adjoint equation as:

$$-\frac{\partial \lambda}{\partial t} = \frac{\partial}{\partial z} \left( K \frac{\partial \lambda}{\partial z} \right) \quad (19)$$

310 Deposition velocities are included in the first layer as part of the boundary conditions. The same numerical scheme can be used for adjoint integrations by excluding only the emissions. Equation (20) is evolved to the next time step by applying the following operator,

$$C^{n+1} = (LHS)^{-1} [(RHS)C^n + E^n] \quad (20)$$

315 where *LHS* and *RHS* are tri-diagonal left hand side and right hand side matrices in a Crank-Nicholson discretization, respectively. Therefore, the discrete adjoint operator is,

$$\lambda^n = (RHS)^T (LHS)^{-T} \lambda^{n+1} \quad (21)$$

For vertical diffusion, discrete and continuous adjoints produce nearly identical results. We use the continuous approach in the present implementation. The gradients of the cost function with respect to emissions can be calculated from the adjoint variables during backward integrations:

320 
$$\frac{\partial J}{\partial E^n} = \left( \frac{\partial C^{n+1}}{\partial E^n} \right)^T \left( \frac{\partial J}{\partial C^{n+1}} \right) = (LHS)^{-1} \lambda^{n+1} \quad (22)$$

325 Note that the required factorization in Equation (23) is already carried out for continuous adjoint integration. Therefore, calculation of the gradient of the cost function with respect to emissions of each

species is accomplished by the minimal cost of one additional back-substitution in the modified tri-diagonal solver used in the adjoint integration.

330 Figure 6 compares BF and adjoint sensitivity fields for sensitivities of ozone at the surface with respect to surface NO emissions when simulations include only chemistry and vertical diffusion. As the accuracy of chemistry adjoints has been previously verified, the agreement shown in Figure 6 serves as validation of both the adjoint of vertical diffusion and calculation of emission gradients.

335 **Horizontal diffusion adjoint.** In CMAQ species undergo horizontal diffusion according to the following equation,

$$\frac{\partial C}{\partial t} = \frac{1}{\rho} \frac{\partial}{\partial x} \left( \rho K \frac{\partial C}{\partial x} \right) \quad (23)$$

the continuous adjoint of which is,

340

$$-\frac{\partial \lambda}{\partial t} = \frac{\partial}{\partial x} \left( \rho K \frac{\partial (\lambda/\rho)}{\partial x} \right) \quad (24)$$

The horizontal diffusion operator is symmetrical, and therefore, self-adjoint. As a result: (a) the same numerical scheme can be used to horizontally diffuse concentrations and adjoints in forward and backward simulations; and (b) continuous and discrete horizontal diffusion adjoints are identical. We use the same subroutine for horizontal diffusion of adjoints with an internal “decoupling” from (division by) densities (see Table 2). Adjoint and BF sensitivity fields show good agreement in Figure 7 where only horizontal diffusion in one direction is included in the simulations and sensitivities of final ozone at the 21<sup>st</sup> x-cross section with respect to initial ozone at the 20<sup>th</sup> column are shown.

350 **Overall implementation.** In the present implementation, forward and backward (and DDM) models are run as separate, independent models. For executing adjoint and DDM models, one first needs to once carry out the forward simulation and store the generated checkpoint files. For subsequent adjoint

(and DDM) simulations, however, execution of the forward model is not required, as the same checkpoint files can be re-used. This leads to significant computational savings when multiple backward  
355 simulations are performed. In general, the order in which processes are called during the backward simulation is reverse of that in the forward simulation (Table 2). As only chemistry requires knowledge of concentrations in the current implementation, checkpoints are written and read before each chemistry call. However, transported air densities are written to checkpoint files after each horizontal advection scheme in the forward mode, and read before each vertical advection scheme in the backward  
360 simulation.

In summary, validation of full adjoint results (including all processes) with forward sensitivity fields (BF or DDM) is possible only for a few sensitivity coefficients. Validation of the adjoint of isolated processes through comparison with forward sensitivity fields can be carried out for a larger number of  
365 points-of-comparison (Figures 3-7), and provides for a more robust verification procedure. Full model results are also in good agreement with BF sensitivities as shown in Figure 8 for few select points and types of sensitivity coefficients.

**Computational efficiency.** The original CMAQ provides 3 options for chemical solvers in Euler  
370 Backward Iterative (EBI), a vectorized Gear solver (SMVGEAR), and ROS3 from the family of Rosenbrock solvers. With the implementation of KPP, users of CMAQ-ADJ have access to 5 Rosenbrock and 4 Runge-Kutta solvers that differ in the order of integration method. Unlike the original implementation of ROS3 in CMAQ, KPP implementation does not employ cell blocking for improved performance on vectorized machines. Table 1 shows comparison of computational times for forward,  
375 DDM, and adjoint models with various solvers. All tests are carried out for a 1-day simulation for a  $45 \times 46 \times 18$  computational domain with 36 km horizontal resolution. In these simulations, the CB-IV chemical mechanism is used. Computational times for forward runs are normalized to the simulation time for the model with CMAQ's EBI solver. Overall the EBI solver provides the fast simulation times,

however, it has the lowest accuracy. For similar tolerance limits all other solvers show similarly good  
 380 accuracy. Rosenbrock solvers, however, outperform other groups in these tests that are carried out on  
 non-vectorized machines (Figure 2). Also shown in Table 1 are relative costs of forward and backward  
 sensitivity calculation. Backward calculations require at least twice the computational time as forward  
 calculations (significantly more for Runge-Kutta solvers), as in the two-level checkpointing scheme, a  
 second-level forward integration is performed for retrieval of concentrations at the internal time steps in  
 385 between checkpoint intervals. Finally, note that the relative costs in Table 1 are for a single  
 receptor/cost function (in adjoint mode) or source/sensitivity parameter (in DDM mode). When  
 sensitivities for multiple receptors or sources are calculated simultaneously, the overall cost per  
 receptor/source for both DDM and adjoint simulation is significantly reduced. This is a result of the  
 shared computational cost in matrix factorization among various receptors/sources. The potential saving  
 390 is more substantial for large chemical mechanisms where chemistry integration is a larger contributor to  
 the overall computational cost.

### Applications in receptor-based sensitivity analysis

The adjoint method has been used widely for variational data assimilations and inverse modeling. In  
 395 these applications, the cost function can be defined generally as,

$$\begin{aligned}
 J &= J_{Observations} + J_{Background} \\
 &= \frac{1}{2}(\mathbf{C} - \mathbf{C}_{obs})^T \mathbf{O}^{-1}(\mathbf{C} - \mathbf{C}_{obs}) + \frac{1}{2}(\mathbf{a} - \mathbf{a}^b)^T \mathbf{B}^{-1}(\mathbf{a} - \mathbf{a}^b)
 \end{aligned}
 \tag{25}$$

400 where  $\mathbf{C}_{obs}$  is a set of observed concentrations,  $\mathbf{a}^b$  is an *a priori* (background or initial guess) estimate  
 of inputs, and where  $\mathbf{O}$  and  $\mathbf{B}$  are observation and background error covariance matrices. The cost  
 function consists of two parts: the first part is a measure of model prediction errors, and the second part  
 is a penalty for deviation from a priori estimates of model inputs. In typical applications the adjoint  
 method is used to calculate the gradients of the cost function with respect to initial concentrations (for



405 data assimilation applications) or model parameters such as emissions (for inverse modeling applications). These gradients are then used in an iterative optimization algorithm in order to minimize the cost function, which reduces the mismatch of model predictions and observations is reduced by adjusting the inputs (e.g. emissions) within a reasonable range. Variational methods provide an important approach for constraining emissions of various species on a spatially resolved basis (36).

410

The adjoint method is a powerful tool for receptor-oriented, sensitivity analysis. As a receptor-based method, adjoint sensitivity analysis is particularly suitable for addressing policy problems. Hakami et al. (64) used the adjoint of a CTM for ozone nonattainment sensitivity analysis over the continental United States. They demonstrated that the adjoint method is a powerful framework for formal analysis of interstate, trans-boundary, and intercontinental transport of pollution. Similar approach can be taken to analyze local nonattainment. Here, we briefly describe a few other potential applications for adjoint sensitivity analysis at regional scales using the adjoint of CMAQ. These applications differ only in the definition of the cost function.

420 **Population exposure analysis.** If the cost function is defined as a population exposure metric, then the resulting sensitivities identify the most influential parameters (emissions) affecting population exposure,

$$J = \sum_{x,y,t} [P \times (C_i - \gamma)]_{x,y,t} \quad (26)$$

425  $\gamma$  represents an exposure threshold, and  $P$  is the population at each location. Note that Equation (26) can be extended to include dose-response relationships for one or multiple pollutants to represent public health risks. As a target-based method, adjoint analysis can identify the most influential emission sources that contribute to the overall exposure/risk metric (e.g., Figure 9). As expected, this definition of the cost function emphasizes areas with large population densities.

430

**Environmental exposure.** A cost function similar to that in Equation (26) can be used to quantify environmental stress resulting from increased pollution levels. For example, an environmental exposure metric based on the W-126 function can be defined to quantify the impact of increased ozone on crops and vegetation (65, 66),

435

$$J = \sum_{x,y,t} \left[ \frac{C_i}{1 + 4403 \exp(-216C_i)} \right]_{x,y,t} \quad (27)$$

Using the above as the cost function in adjoint analysis, corresponding (emission) gradients can be calculated (Figure 10). Areas of significant gradients (right panel) indicate sources where emission control can result in largest reductions in the cost function (left panel). The adjoint method affords users the flexibility to combine environmental and public health metrics in a single cost function for integrated analysis of air pollution effects.

440

**Effect of temperature variation on air pollution levels.** In a manner similar to the calculation of emission gradients, the sensitivity of the cost function with respect to changes in temperature can be calculated,

445

$$\frac{\partial J}{\partial T^n} = \left( \frac{\partial C^{n+1}}{\partial T} \right)^T \left( \frac{\partial J}{\partial C^{n+1}} \right) = \left( \frac{\partial k^n}{\partial T} \right)^T \left( \frac{\partial C^{n+1}}{\partial k^n} \right)^T \lambda^{n+1} \quad (28)$$

As written, Equation (28) describes only the effect of temperature on the cost function via chemistry. Changes in temperatures will also affect biogenic (and anthropogenic) emissions. The results of applying Equation (28) in the adjoint analysis for population and environmental exposures above [Equations (26) and (27)] are shown in Figure 11. It is interesting that temperature gradients show significant spatial distributions, something that is possible to capture only in a receptor-oriented method, i.e., adjoint sensitivity analysis. Spatial distributions such as those in Figure 12 can be used in conjunction with results from regional climate studies to formally quantify the impact of future climate

450

455

conditions on regional air quality. These gradients can also be used to quantify contributions to the uncertainties in future (or current) air quality from uncertainty/variability in regional temperatures.

## Acknowledgements

460 This work was supported by National Science Foundation award NSF ITR AP&IM 0205198 and by funding from the Jet Propulsion Laboratory. The work of A. Sandu and K. Singh was also supported by the Houston Advanced Research Council through the award H59/2005.

## References

- 465 1- Dickinson, R. P.; Gelinas, R. J. Sensitivity analysis of ordinary differential equation systems - Direct method. *J Comput Phys* **1976**, 21, 123-143.
- 2- Dunker, A. M. Efficient calculation of sensitivity coefficients for complex atmospheric models. *Atmos Environ* **1981**, 15, 1155-1161.
- 3- Dunker, A. M. The Decoupled direct method for calculating sensitivity coefficients in chemical  
470 kinetics. *J Chem Phys* **1984**, 81, 2385-2393.
- 4- Yang, Y. J.; Wilkinson, J. G.; Russell, A. G. Fast, direct sensitivity analysis of multidimensional photochemical models. *Environ Sci Technol* **1997**, 31, 2859-2868.
- 5- He, S.; Carmichael, G. R.; Sandu, A.; Hotchkiss, B.; Damian-Iordache, V. Application of ADIFOR for air pollution model sensitivity studies. *Environ Modell Softw* **2000**, 15, 549-557.
- 475 6- Dunker, A. M.; Yarwood, G.; Ortman, J. P.; Wilson, G. M. The decoupled direct method for sensitivity analysis in a three-dimensional air quality model - Implementation, accuracy, and efficiency. *Environ Sci Technol* **2002**, 36, 2965-2976.
- 7- Hakami, A.; Odman, M. T.; Russell, A. G. High-order, direct sensitivity analysis of multidimensional air quality models. *Environ Sci Technol* **2003**, 37, 2442-2452.
- 480 8- Cacuci, D. G.; Schlesinger, M. E. On the application of the adjoint method of sensitivity analysis to problems in the atmospheric sciences. *Atmosfera* **1994**, 7, 47-59.

- 9- Marchuk, G. I.; Shutyaev, V.; Bocharov, G. Adjoint equations and analysis of complex systems: Application to virus infection modelling. *J Comput Appl Math* **2005**, 184, 177-204.
- 10- Marchuk, G. I. *Numerical Solution of the Problems of the Dynamics of the Atmosphere and the Ocean* (in Russian); Gidrometeoizdat: St. Petersburg, 1974.
- 11- Cacuci, D. G. Sensitivity theory for nonlinear systems .1. Nonlinear functional analysis approach. *J Math Phys* **1981**, 22, 2794-2802.
- 12- Cacuci, D. G. Sensitivity theory for Nonlinear systems .2. Extensions to additional classes of responses. *J Math Phys* **1981**, 22, 2803-2812.
- 13- Marchuk, G. I. *Mathematical models in environmental problems*; North-Holland ; sole distributors for the U.S.A and Canada, Elsevier Science Pub. Co.: Amsterdam ; New York, New York, 1986.
- 14- Cacuci, D. G.; Ionescu-Bujor, M. Deterministic local sensitivity analysis of augmented systems - I: Theory. *Nucl Sci Eng* **2005**, 151, 55-66.
- 15- Cacuci, D. G.; Ionescu-Bujor, M.; Navon, I. M. *Sensitivity and Uncertainty Analysis*; Chapman & Hall/CRC Press: Boca Raton, 2003.
- 16- Hall, M. C. G.; Cacuci, D. G.; Schlesinger, M. E. Sensitivity analysis of a radiative-convective model by the adjoint method. *J Atmos Sci* **1982**, 39, 2038-2050.
- 17- Hall, M. C. G.; Cacuci, D. G. Physical interpretation of the adjoint functions for sensitivity analysis of atmospheric models. *J Atmos Sci* **1983**, 40, 2537-2546.
- 18- Ledimet, F. X.; Talagrand, O. Variational algorithms for analysis and assimilation of meteorological observations - Theoretical aspects. *Tellus A* **1986**, 38, 97-110.
- 19- Talagrand, O.; Courtier, P. Variational assimilation of meteorological observations with the adjoint vorticity equation .1. Theory. *Q J Roy Meteor Soc* **1987**, 113, 1311-1328.
- 20- Courtier, P.; Talagrand, O. Variational assimilation of meteorological observations with the adjoint vorticity equation .2. Numerical results. *Q J Roy Meteor Soc* **1987**, 113, 1329-1347.
- 21- Navon, I. M. Practical and theoretical aspects of adjoint parameter estimation and identifiability in meteorology and oceanography. *Dynam Atmos Oceans* **1998**, 27, 55-79.

- 22- Elbern, H.; Schmidt, H.; Ebel, A. Variational data assimilation for tropospheric chemistry modeling.  
510 *J Geophys Res-Atmos* **1997**, 102, 15967-15985.
- 23- Elbern, H.; Schmidt, H. A four-dimensional variational chemistry data assimilation scheme for Eulerian chemistry transport modeling. *J Geophys Res-Atmos* **1999**, 104, 18583-18598.
- 24- Elbern, H.; Schmidt, H.; Talagrand, O.; Ebel, A. 4D-variational data assimilation with an adjoint air quality model for emission analysis. *Environ Modell Softw* **2000**, 15, 539-548.
- 515 25- Elbern, H.; Schmidt, H. Ozone episode analysis by four-dimensional variational chemistry data assimilation. *J Geophys Res-Atmos* **2001**, 106, 3569-3590.
- 26- Vukicevic, T.; Hess, P. Analysis of tropospheric transport in the Pacific Basin using the adjoint technique. *J Geophys Res-Atmos* **2000**, 105, 7213-7230.
- 27- Menut, L.; Vautard, R.; Beekmann, M.; Honore, C. Sensitivity of photochemical pollution using the  
520 adjoint of a simplified chemistry-transport model. *J Geophys Res-Atmos* **2000**, 105, 15379-15402.
- 28- Vautard, R.; Beekmann, M.; Menut, L. Applications of adjoint modelling in atmospheric chemistry: sensitivity and inverse modelling. *Environ Modell Softw* **2000**, 15, 703-709.
- 29- Menut, L. Adjoint modeling for atmospheric pollution process sensitivity at regional scale. *J Geophys Res-Atmos* **2003**, 108 (D17), 8562, doi:10.1029/2002JD002549.
- 525 30- Sandu, A.; Daescu, D. N.; Carmichael, G. R.; Chai, T. F. Adjoint sensitivity analysis of regional air quality models. *J Comput Phys* **2005**, 204, 222-252.
- 31- Hakami, A.; Henze, D. K.; Seinfeld, J. H.; Chai, T.; Tang, Y.; Carmichael, G. R.; Sandu, A. Adjoint inverse modeling of black carbon during the Asian Pacific Regional Aerosol Characterization Experiment. *J Geophys Res-Atmos* **2005**, 110, D14301, doi:10.1029/2004JD005671.
- 530 32- Chai, T. F.; Carmichael, G. R.; Sandu, A.; Tang, Y. H.; Daescu, D. N. Chemical data assimilation of Transport and Chemical Evolution over the Pacific (TRACE-P) aircraft measurements. *J Geophys Res-Atmos* **2006**, 111, D02301, doi:10.1029/2005JD005883.
- 33- Mallet, V.; Sportisse, B. A comprehensive study of ozone sensitivity with respect to emissions over Europe with a chemistry-transport model. *J Geophys Res-Atmos* **2005**, 110, D22302,  
535 doi:10.1029/2005JD006234.

- 34- Quelo, D.; Mallet, V.; Sportisse, B. Inverse modeling of NO<sub>x</sub> emissions at regional scale over northern France: Preliminary investigation of the second-order sensitivity. *J Geophys Res-Atmos* **2005**, 110, D24310, doi:10.1029/2005JD006151.
- 35- Martien, P. T.; Harley, R. A. Adjoint sensitivity analysis for a three-dimensional photochemical model: Implementation and method comparison. *Environ Sci Technol* **2006**, 40, 2663-2670.
- 540 36- Martien, P. T.; Harley, R. A. Adjoint sensitivity analysis for a three-dimensional photochemical model: Application to Southern California. *Environ Sci Technol* **2006**, 40, 4200-4210.
- 37- Nester, K.; Panitz, H. J. Sensitivity analysis by the adjoint chemistry transport model DRAIS for an episode in the Berlin Ozone (BERLIOZ) experiment. *Atmos Chem Phys* **2006**, 6, 2091-2106.
- 545 38- Muller, J. F.; Stavrou, T. Inversion of CO and NO<sub>x</sub> emissions using the adjoint of the IMAGES model. *Atmos Chem Phys* **2005**, 5, 1157-1186.
- 39- Stavrou, T.; Muller, J. F. Grid-based versus big region approach for inverting CO emissions using Measurement of Pollution in the Troposphere (MOPITT) data. *J Geophys Res-Atmos* **2006**, 111, D15304, doi:10.1029/2005JD006896.
- 550 40- Meirink, J. F.; Eskes, H. J.; Goede, A. P. H. Sensitivity analysis of methane emissions derived from SCIAMACHY observations through inverse modelling. *Atmos Chem Phys* **2006**, 6, 1275-1292.
- 41- Henze, D. K.; Hakami, A.; Seinfeld, J. H. Development of the adjoint of GEOS-Chem. *Atmos Chem Phys*, in press, 2007.
- 42- Byun, D. W.; Ching, J. K. S. Science algorithms of the EPA Models-3 Community Multiscale Air Quality (CMAQ) Modeling System, U. S. Environmental Protection Agency, USEPA/600/R-99/030; Research Triangle Park, NC, 1999.
- 555 43- Byun, D. W.; Schere, K. L. Review of the governing equations, computational algorithms, and other components of the Models-3 Community Multiscale Air Quality (CMAQ) modeling system. *Applied Mechanics Reviews* **2006**, 59, 51-77.
- 560 44- Seinfeld, J. H.; Pandis, S. N. *Atmospheric Chemistry and Physics : From Air Pollution to Climate Change*; 2nd ed.; J. Wiley: Hoboken, N.J., 2006.
- 45- Jacobson, M. Z. *Fundamentals of Atmospheric Modeling*; 2nd ed.; Cambridge University Press: New York, 2005.

- 565 46- Navon, I. M.; Zou, X.; Derber, J.; Sela, J. Variational data assimilation with an adiabatic version of the NMC spectral model. *Mon Weather Rev* **1992**, 120, 1433-1446.
- 47- Sirkes, Z.; Tziperman, E. Finite difference of adjoint or adjoint of finite difference? *Mon Weather Rev* **1997**, 125, 3373-3378.
- 48- Cohan, D. S.; Hu, Y.; Hakami, A.; Odman, M. T.; Russell, A. G. Implementation of a direct sensitivity method into CMAQ, Models-3 Annual Conference, Chapel Hill, NC, 2002.
- 570 49- Damian, V.; Sandu, A.; Damian, M.; Potra, F.; Carmichael, G. R. The kinetic preprocessor KPP - a software environment for solving chemical kinetics. *Comput Chem Eng* **2002**, 26, 1567-1579.
- 50- Daescu, D.; Carmichael, G. R.; Sandu, A. Adjoint implementation of Rosenbrock methods applied to variational data assimilation problems. *J Comput Phys* **2000**, 165, 496-510.
- 51- Sandu, A.; Sander, R. Technical note: Simulating chemical systems in Fortran90 and Matlab with the Kinetic PreProcessor KPP-2.1. *Atmos Chem Phys* **2006**, 6, 187-195.
- 575 52- Sandu, A.; Daescu, D. N.; Carmichael, G. R. Direct and adjoint sensitivity analysis of chemical kinetic systems with KPP: Part I - theory and software tools. *Atmos Environ* **2003**, 37, 5083-5096.
- 53- Daescu, D. N.; Sandu, A.; Carmichael, G. R. Direct and adjoint sensitivity analysis of chemical kinetic systems with KPP: II - Numerical validation and applications. *Atmos Environ* **2003**, 37, 5097-5114.
- 580 54- Hairer, E.; Wanner G. *Solving Ordinary Differential Equations II. Stiff and Differential-Algebraic Problems*; Springer: Berlin, 1991.
- 55- Sandu, A.; Verwer, J. G.; Blom, J. G.; Spee, E. J.; Carmichael, G. R.; Potra, F. A. Benchmarking stiff ODE solvers for atmospheric chemistry problems .2. Rosenbrock solvers. *Atmos Environ* **1997**, 31, 3459-3472.
- 585 56- Miehe, P; Sandu, A. Forward, tangent linear, and adjoint Runge-Kutta methods in KPP-2.2. *Lecture Notes in Computer Science* **2006**, 3993, 120-127.
- 57- Jacobson, M. Z.; Turco, R. P. Smvgear - a Sparse-Matrix, Vectorized Gear code for atmospheric models. *Atmos Environ* **1994**, 28, 273-284.
- 590 58- Hertel, O.; Berkowicz, R.; Christensen, J.; Hov, O. Test of two numerical schemes for use in atmospheric transport chemistry models. *Atmos Environ* **1993**, 27, 2591-2611.

- 59- Griewank, A.; Walther, A. Algorithm 799: Revolve: An implementation of checkpointing for the reverse or adjoint mode of computational differentiation. *Acm T Math Software* **2000**, 26, 19-45.
- 595 60- Colella, P.; Woodward, P. R. The Piecewise Parabolic Method (PPM) for gas dynamical simulations. *J Comput Phys* **1984**, 54, 174-201.
- 61- Vukicevic, T.; Steyskal, M.; Hecht, M. Properties of advection algorithms in the context of variational data assimilation. *Mon Weather Rev* **2001**, 129, 1221-1231.
- 62- Liu, Z.; Sandu, A. Analysis of discrete adjoints for upwind numerical schemes. *Lect Notes Comput Sc* **2005**, 3515, 829-836.
- 600 63- Thuburn, J.; Haine, T. W. N. Adjoint of nonoscillatory advection schemes. *J Comput Phys* **2001**, 171, 616-631.
- 64- Hakami, A.; Seinfeld, J. H.; Chai, T. F.; Tang, Y. H.; Carmichael, G. R.; Sandu, A. Adjoint sensitivity analysis of ozone nonattainment over the continental United States. *Environ Sci Technol* **2006**, 40, 3855-3864.
- 605 65- Lefohn, A. S.; Runeckles, V. C. Establishing standards to protect vegetation - Ozone exposure dose considerations. *Atmos Environ* **1987**, 21, 561-568.
- 66- U. S. EPA. Air quality criteria for ozone and related photochemical oxidants, U. S. Environmental Protection Agency, EPA/600/P-93/004bF, Research Triangle Park, NC, 1996.

610



## FIGURE CAPTIONS

Figure 1: Comparison between BF (left) and DDM (right) semi-normalized sensitivities of ozone with respect to initial ozone concentration after 6 hours of simulation. BF sensitivities are central difference approximations unless specified otherwise.

615 Figure 2: Work-precision diagrams for day-long simulations with various CMAQ (black) and KPP solvers (Rosenbrock in red, and Runge-Kutta in blue). Significant digit accuracy (SDA) for each species is defined as  $SDA_i = -\log(RMSRE_i)$ , where RMSRE is the root mean square of relative error in comparison with a reference solution. Diagrams are shown for the overall SDA (minimum across all species). Simulations with default/recommended settings are indicated by enlarged, green markers. For  
620 this application, most Rosenbrock solvers fall in the desirable performance region.

Figure 3: Comparison of Adjoint and BF sensitivities of final ozone concentration with respect to initial NO concentration; chemistry-only simulations are carried out for 6 hours.

Figure 4: Comparison of various BF with adjoint sensitivity of ozone at the 20<sup>th</sup> column with respect to initial ozone at the 20<sup>th</sup> column. Only horizontal advection in the x direction included in the simulations.

625 DDM sensitivity shows reasonable agreement with adjoint.

Figure 5: Simulations with only vertical advection for calculation of the sensitivities of surface ozone with respect to initial surface ozone.

Figure 6: Simulations with only chemistry and vertical diffusion, normalized sensitivities of surface ozone with respect to surface emissions of NO.

630 Figure 7: Simulations with only horizontal diffusion in x-direction for calculation of ozone sensitivities at the 21<sup>st</sup> column with respect to initial ozone at 20<sup>th</sup> column.

Figure 8: Full model simulations, sensitivities of surface ozone with respect to surface NO initial concentrations (left) and emissions (right) for selected locations.

635 Figure 9: Spatial distribution of the cost function for population exposure (left) and associated gradients with respect to  $\text{NO}_x$  emissions (right). Values are normalized to the total cost function and presented in percent. Exposure threshold is 60 ppb.

Figure 10: Spatial distribution of the cost function for W-126 metric of vegetation exposure from ozone (left) and associated gradients with respect to  $\text{NO}_x$  emissions (right). Values are normalized to the total cost function and presented in percent.

640 Figure 11: Temperature gradients of the population exposure to ozone (left) and W-126 metric (right). Values are integrated for the duration of the episode, normalized to the total cost function, and presented in percent.

Table1. Comparison of computational times for the forward, DDM and adjoint models with various chemical solvers at the default/recommended settings.

Solver <sup>1</sup>	Normalized computational times <sup>2</sup>		
	Forward Model <sup>3</sup>	DDM <sup>4,5</sup>	Adjoint <sup>4</sup>
CMAQ-EBI	1.00	-	-
CMAQ-ROS3	2.10	-	-
CMAQ-SMVGEAR	3.69	-	-
KPP-ROS2	1.59	1.88	2.02
KPP-ROS3	1.08	1.96	2.02
KPP-ROS4	1.18	2.11	2.11
KPP-RODAS3	0.96	2.12	2.09
KPP-RODAS4	1.18	2.39	2.18
KPP-RADAU-2A	2.08	7.81	7.87
KPP-LOBATTO	2.66	7.93	7.25
KPP-GAUSS	2.66	8.13	5.41
KPP-RADAU-1A	1.99	7.60	7.96

1- For description of solvers see 55-58. 2- All simulations are carried out sequentially for 24-hours, on 64-bit, 2.0 GHz dual-core Opteron processors. 3- Values are normalized to forward simulation with EBI solver. 4- Values are normalized to the forward simulation with the same solver. 5- Values include the time required for concentration integrations.

Table 2. Forward and backward simulation schemes in CMAQ.

Forward Model	Adjoint Model
INIT (t=0)	INIT (t=tF)
DO (Synchronization steps)	DO (Synchronization steps)
DO (Advection steps)	DO (Advection steps)
V-DIFF	FORCE-ADJ
COUPLE	NEXTIME (-TSTEP)
H-ADV	READ CHECKPOINT (CONC)
WRITE CHECKPOINT (Density)	CHEM-ADJ
V-ADV	H-DIFF-ADJ
H-DIFF	READ CHECKPOINT (Density)
DECOUPLE	DECOUPLE
WRITE CHECKPOINT (CONC)	V-ADV-ADJ
CHEM	H-ADV-ADJ
NEXTIME (TSTEP)	COUPLE
END DO	V-DIFF-ADJ
WRITE CONC	END DO
END DO	WRITE ADJ
	END DO

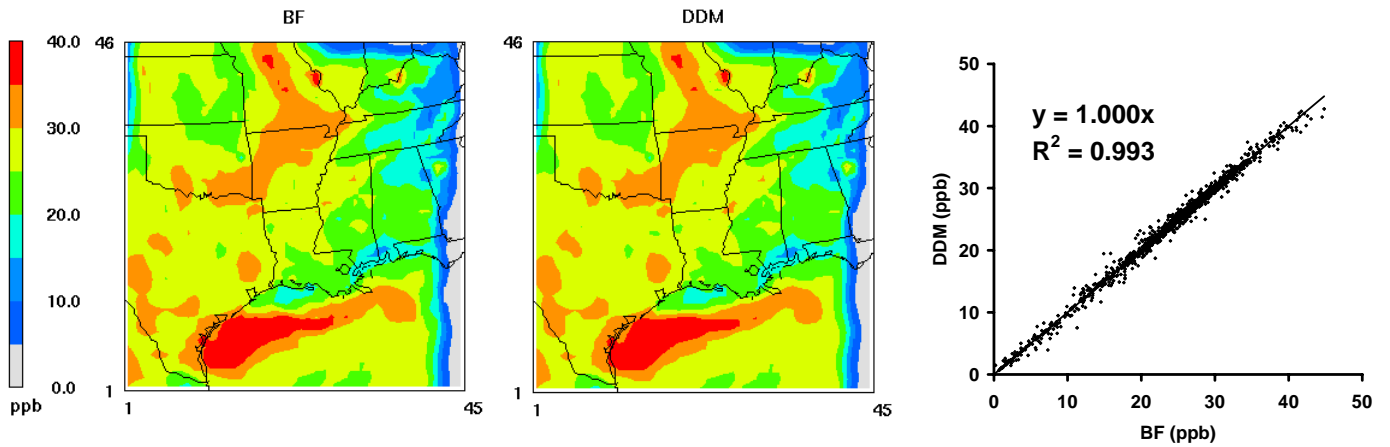


Figure 1: Comparison between BF (left) and DDM (right) semi-normalized sensitivities of ozone with respect to initial ozone concentration after 6 hours of simulation. BF sensitivities are central difference approximations unless specified otherwise.

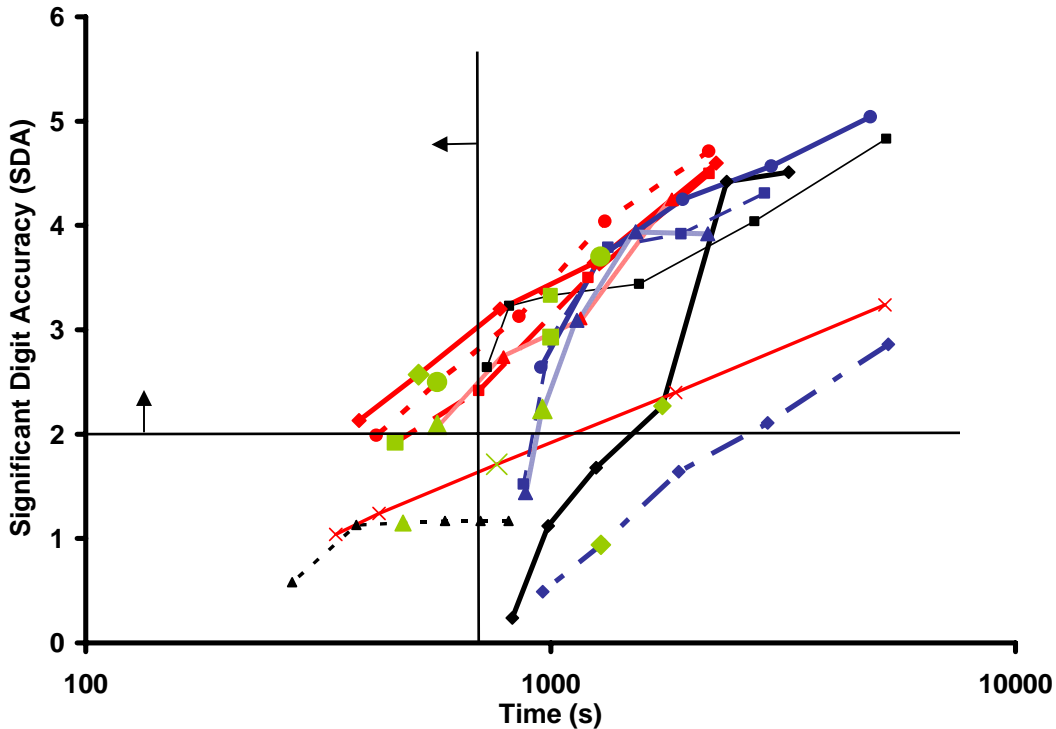


Figure 2: Work-precision diagrams for day-long simulations with various CMAQ (black) and KPP solvers (Rosenbrock in red, and Runge-Kutta in blue). Significant digit accuracy (SDA) for each species is defined as  $SDA_i = -\log(RMSRE_i)$ , where RMSRE is the root mean square of relative error in comparison with a reference solution. Diagrams are shown for the overall SDA (minimum across all species). Simulations with default/recommended settings are indicated by enlarged, green markers. For this application, most Rosenbrock solvers fall in the desirable performance region.

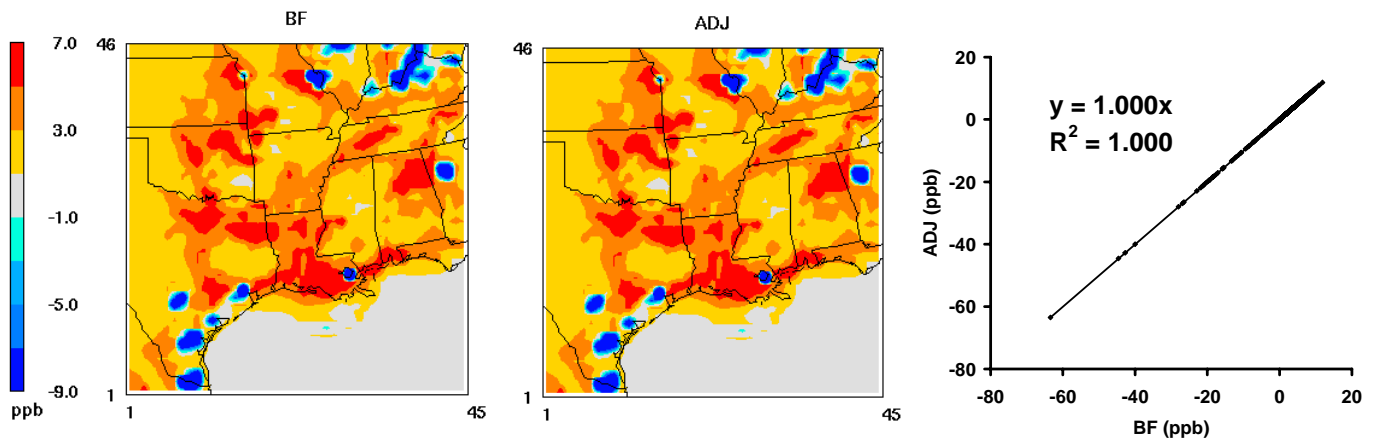


Figure 3: Comparison of adjoint and BF sensitivities of final ozone concentrations with respect to initial NO concentrations; chemistry-only simulations are carried out for 6 hours.

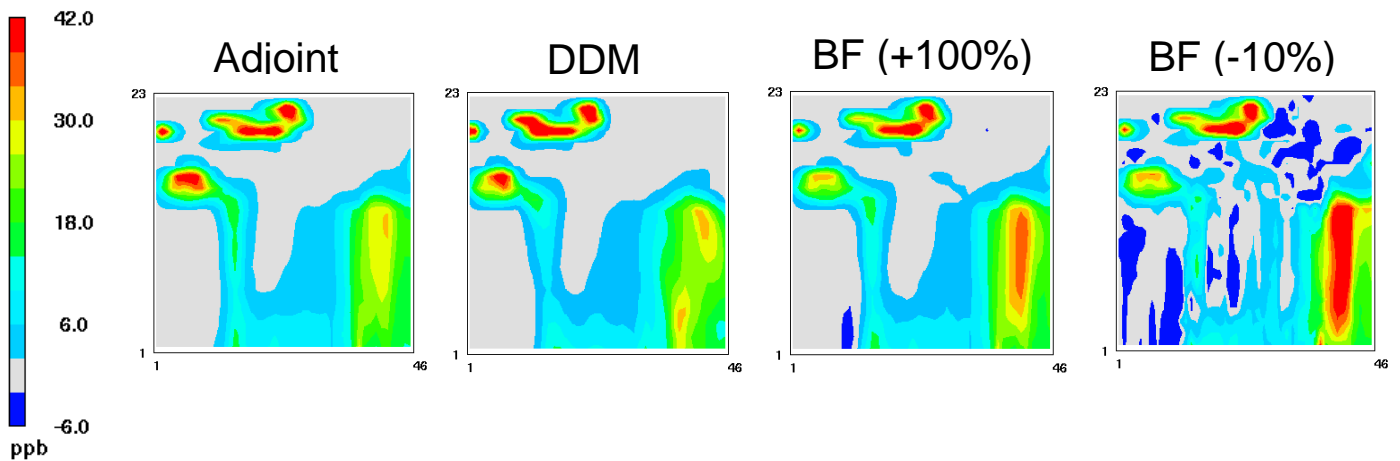


Figure 4: Comparison of BF and adjoint sensitivities of ozone at the 20<sup>th</sup> column with respect to initial ozone at the 20<sup>th</sup> column. Only horizontal advection in the x-direction is included in the simulations. DDM sensitivity shows reasonable agreement with the adjoint.

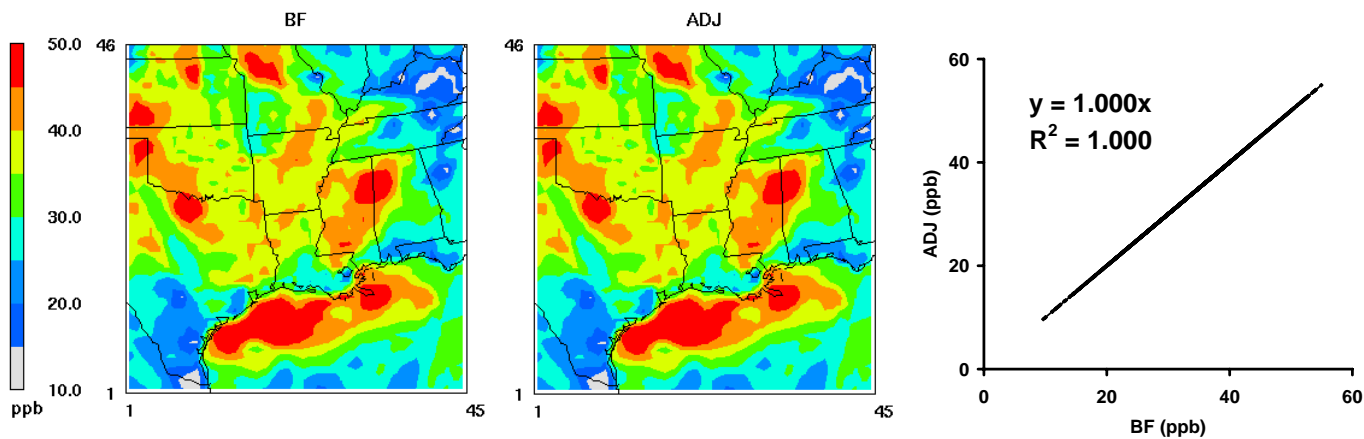


Figure 5: Simulations with only vertical advection for calculation of the normalized sensitivities of surface ozone with respect to initial surface ozone.

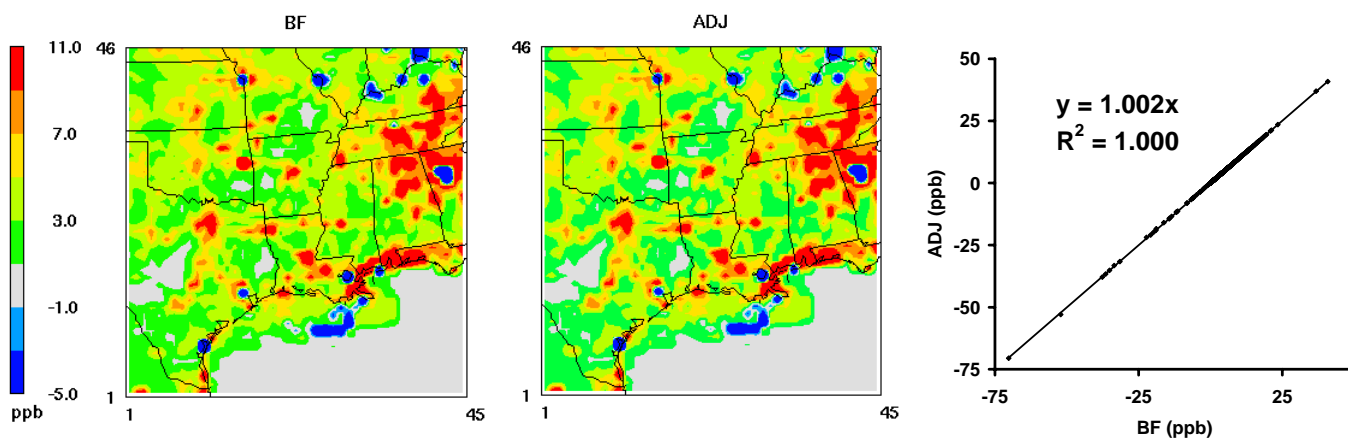


Figure 6: Simulations with only chemistry and vertical diffusion, normalized sensitivities of surface ozone with respect to surface emissions of NO.

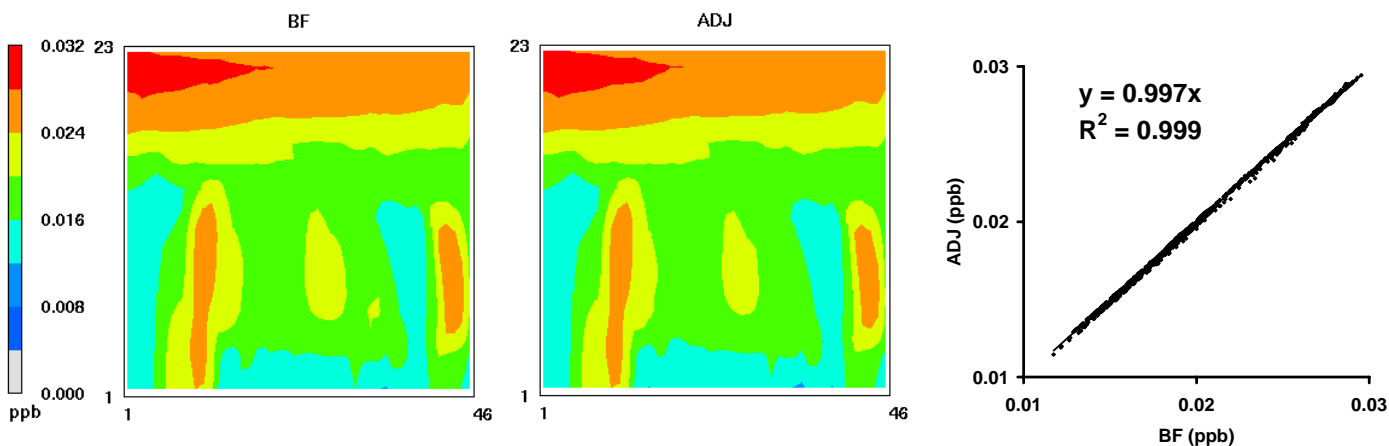


Figure 7: Simulations with only horizontal diffusion in x-direction for calculation of normalized ozone sensitivities at the 21<sup>st</sup> column with respect to initial ozone at 20<sup>th</sup> column.

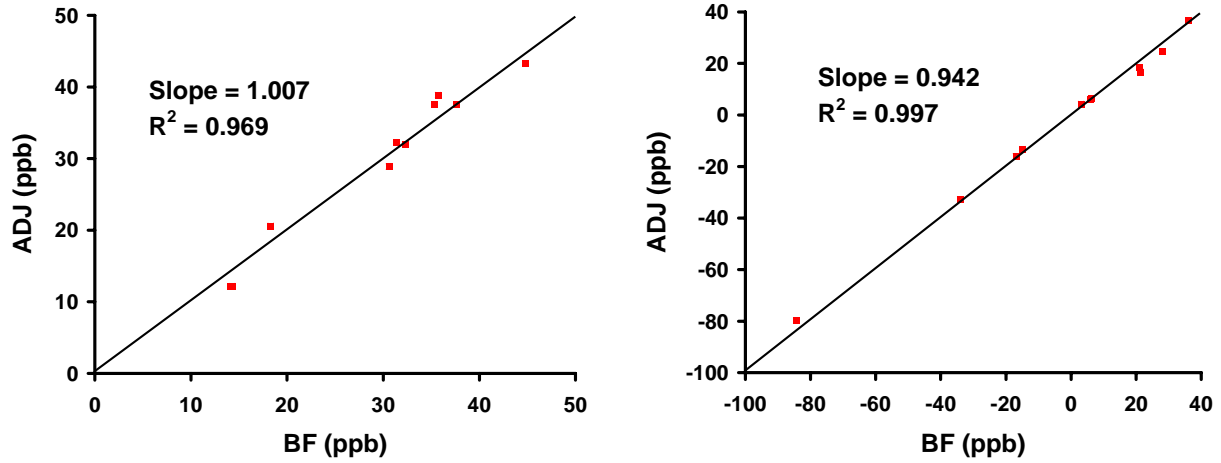


Figure 8: Full model simulations, sensitivities of surface ozone with respect to surface ozone initial concentrations (left) and surface NO emissions (right) for selected locations. Values are shown in comparison to the one-on-one lines.

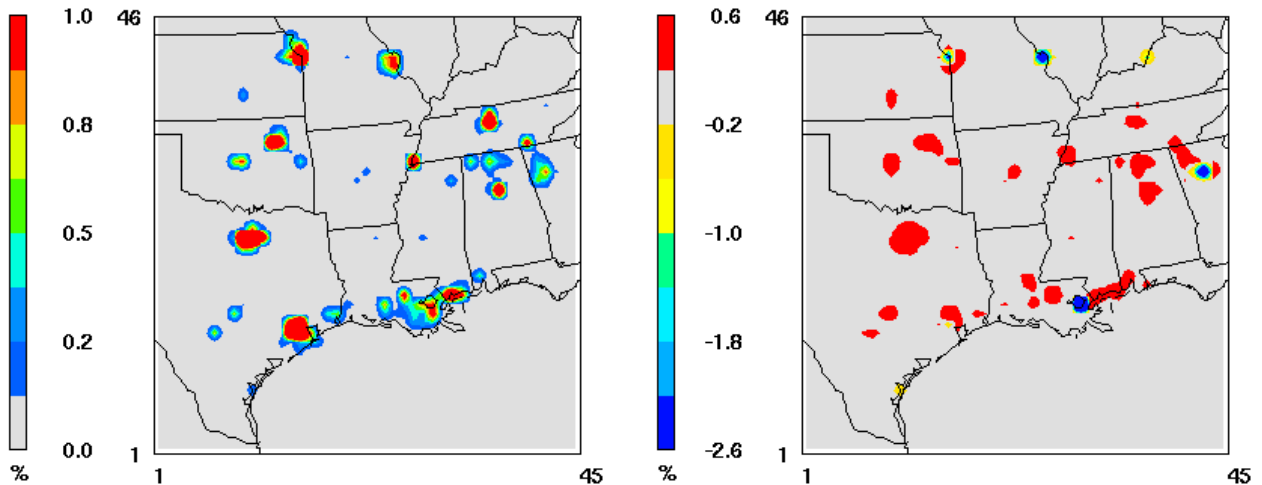


Figure 9: Spatial distribution of the cost function for population exposure (left) and associated gradients with respect to NO<sub>x</sub> emissions (right). Values are normalized to the total cost function and presented in percent. Exposure threshold is 60 ppb.

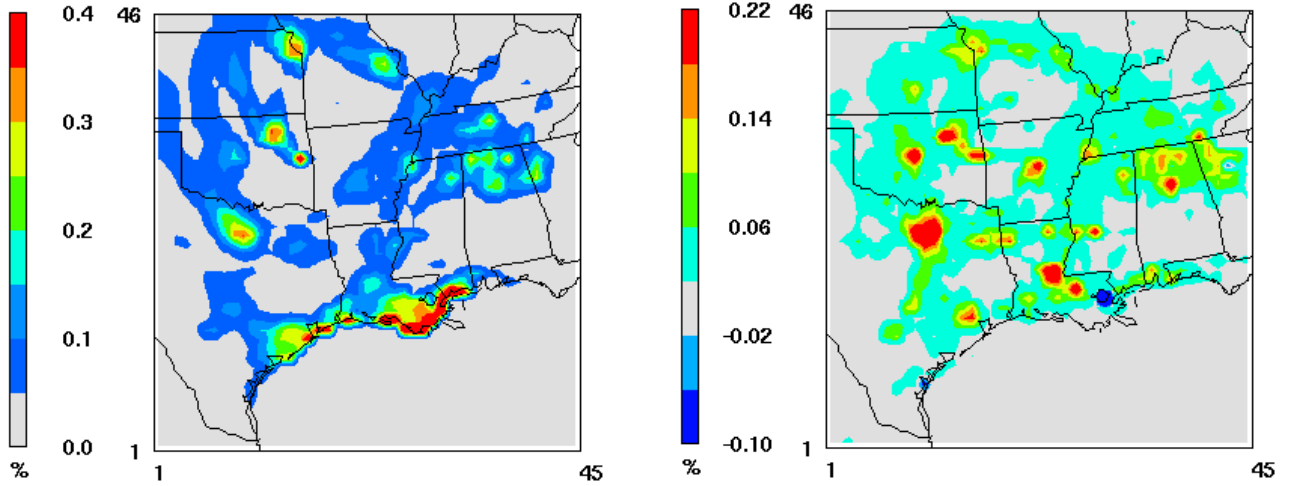


Figure 10: Spatial distribution of the cost function for W-126 metric of vegetation exposure to ozone (left) and associated gradients with respect to NO<sub>x</sub> emissions (right). Values are normalized to the total cost function and presented in percent.

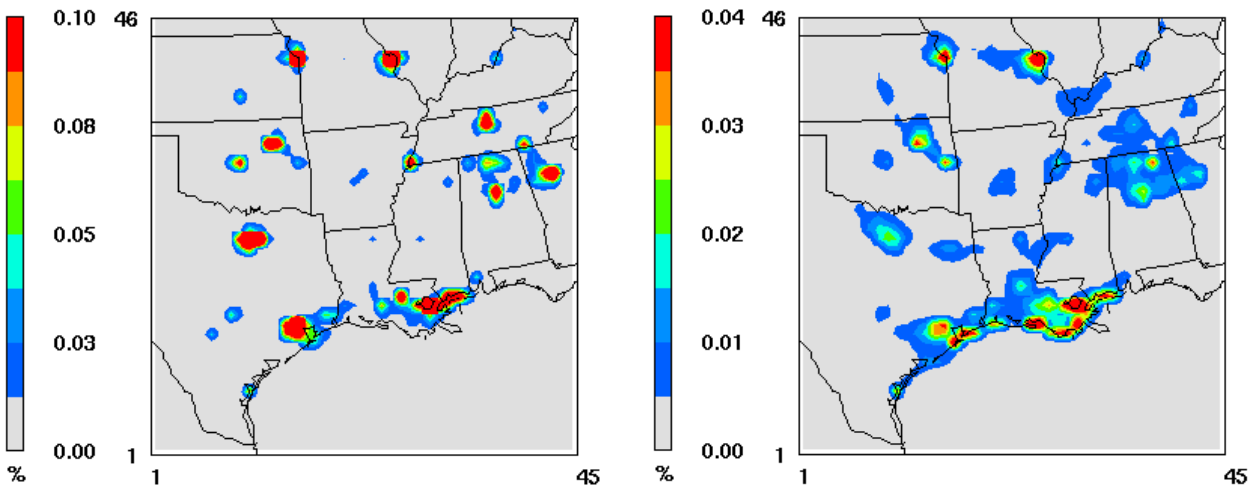


Figure 11: Spatial distribution of the sensitivities of the population exposure to ozone (left) and W-126 metric (right) with respect to local temperatures. Values are integrated for the duration of the episode, normalized to the total cost function, and presented in percent.